Microscopic origin of the macroscopic magnetic properties of TbFeCoN amorphous thin films

C. Bordel, S. Pizzini, J. Vogel, K. Mackay, J. Voiron, R. M. Galéra, and A. Fontaine
Laboratoire de magnétisme Louis Néel (CNRS), associé à l'Université J. Fourier, BP166, 38042 Grenoble Cedex 9, France

P. Auric
DRFMC/Physique/MDTH, CENG, BP 85X, 38041 Grenoble Cedex, France

J. B. Goedkoop and N. B. Brookes
ESRF (European Synchrotron Radiation Facility), BP 220, 38560 Grenoble Cedex, France
(Received 14 March 1997; revised manuscript received 27 May 1997)

The magnetic properties of TbFeCoN amorphous thin films, made by reactive plasma sputtering, were studied on both the macroscopic and microscopic scales, as a function of nitrogen content. Magnetization measurements showed a very important decrease of the compensation temperature for increasing nitrogen concentrations. The element selectivity of x-ray magnetic circular dichroism and Mössbauer spectroscopy enabled the rare earth (RE) magnetic contribution to be discriminated from the transition-metal (TM) contribution. The macroscopic effect of nitrogen insertion in TbFeCo amorphous thin films was found to be mainly due to a progressive opening of the mean angle of the conical distribution of the Tb moments. Mean-field calculations confirm the prominent role of the RE-TM exchange interactions in the magnetic behavior of this system. [S0163-1829(97)01637-8]

I. INTRODUCTION

TbFeCo amorphous alloys are sperimagnetic materials used as magneto-optical recording media since most of the required properties[1] can be fulfilled by using the appropriate concentration of each element. The key points are the stability of the written domains at room temperature (compensation temperature around 300 K), the possibility to reach the writing temperature by laser heating (Curie temperature around 500 K), and the good magnetic and spatial definitions of the domains (perpendicular uniaxial anisotropy and amorphous structure). The recording properties can be improved by using a multilayer system composed of several exchange-coupled layers with different compensation and Curie temperatures,[2,3] which enables one to act on an individual layer by temperature and field modulations. The compensation temperature is an extremely important parameter that ensures the stability of the stored information, since the coercive field is high around this temperature. As already observed,[4,5] this temperature can be decreased by introducing nitrogen. In this way, it is possible to obtain a wide range of compensation temperatures by simply varying the nitrogenation rate. A multilayer-based magneto-optical recording medium could therefore be made from a reduced number of targets.

The decrease of the compensation temperature (T_{comp}), as well as that of the Curie temperature (T_c), upon nitrogenation of TbFeCo films has been observed by magnetization and magneto-optical measurements. As the Tb sublattice magnetization is dominant below T_{comp}, the decrease of T_{comp} must originate either from the enhancement of the Fe sublattice magnetization and/or from the decrease of the Tb sublattice magnetization.

The aim of this work is to present macroscopic magnetic properties obtained for a series of $\mathrm{TbFeCoN}_x$ samples and to understand the microscopic origin of the macroscopic observations related to nitrogen insertion. Its originality lies in the use of x-ray magnetic circular dichroism (XMCD) and Mössbauer spectroscopy as local experimental techniques. The complementarity of these techniques is essential for the study of this sperimagnetic system, in which both the Tb and Fe magnetic moments form noncollinear structures.

XMCD measures the absorption dependence of a ferromagnetic (or ferrimagnetic) material on the helicity of the incoming photons. Since the early experiments of Chen *et al.*[6] at the $L_{2,3}$ edges of Ni, soft x-ray magnetic dichroism has been widely developed and is now a very well established tool to study local magnetic properties.

The selectivity of x-ray-absorption spectroscopy allows, for each atomic species of the probed material, the magnetic polarization of the electronic states of selected symmetry to be investigated. XMCD at the $M_{4,5}$ edges of the rare earths (RE's) can be modeled within the atomic multiplet approach[7,8] and allows $4f$ magnetic moments to be extracted. The $L_{2,3}$ edges of the transition metals (TM's) are still more difficult to be interpreted. A very important development of this spectroscopy has been the formulation of the sum rules[9] which relate the intensities of the total absorption and XMCD spectra to the spin and orbital magnetic $3d$ moments in the ground state.

Previous studies[10,11] showed that XMCD is highly suited for the investigation of the magnetic properties of intermetallic amorphous alloys, as the chemical selectivity of this technique enables the RE and TM sublattices to be independently probed. Note that in amorphous RE-TM alloys, which can form noncollinear magnetic structures, XMCD enables only the mean projected moments (on the total magnetization direction) to be determined. Since the $4f$ magnetic moments can be assumed to have their atomic value, XMCD at the $M_{4,5}$ edges of Tb can give us information about the angular

distribution of the Tb magnetic moments with respect to the total magnetization direction. On the contrary, the TM 3*d* moments are strongly sample dependent, and no similar information can be deduced for the Fe magnetic sublattice from XMCD at the $L_{2,3}$ edges.

For this reason, conversion electron Mössbauer spectroscopy (CEMS) was also performed. This local technique, based on the resonant absorption of γ rays by a Mössbauer nucleus, is known to be a very efficient tool in the study of Fe-based alloys. Among the characteristic parameters that can be deduced from the Fe spectra, the hyperfine field, the isomer shift, and the Mössbauer angle are, respectively, related to the intrinsic Fe magnetic moment, the *s*-electron density at the nucleus, and the angle between the hyperfine field and the incident γ-ray beam. This probe was then used to obtain the mean magnetic structure of the Fe sublattice.

The validity of the assumption coming from the interpretation of the experimental results was tested by using a mean-field analysis.

II. SAMPLE PREPARATION AND CHARACTERIZATION

We have investigated several $Tb_{100-y}(Fe,Co)_yN_x$ alloy thin films, with a constant TbFeCo composition (y is constant) and various nitrogen concentrations x. The films were sputtered on SiO_2 substrates from two $Tb_{24}Fe_{68}Co_8$ facing targets, and covered with 3 nm Al. As nitrogen and argon are cointroduced in the sputtering chamber, the alloy is nitrided during the deposition process. The nitrogen concentration in the sputtering gas is monitored and controlled by modifying the ratio of the nitrogen flow (variable) over the total flow (fixed).

The amorphous structure was checked by x-ray diffraction in a conventional θ-2θ diffractometer. The two peaks detectable on the spectra were identified as (400)-Si and (111)-Al, and so the magnetic alloys do not present any long-range order.

The thickness and RE-TM composition were determined by Rutherford backscattering spectroscopy, with a normally incident beam of 2-MeV α particles. The RE-TM alloy composition was deduced, with an accuracy of 1%, from the relative intensity of the RE and TM peaks (Fe and Co cannot be separated by this technique because of their close masses), and found to be $Tb_{25}(Fe,Co)_{75}$. The thickness, which is related to the width of the peaks, is determined with a 3% accuracy, and is close to 100 nm for all the samples.

Electron probe microanalysis enabled the Co concentration to be estimated at (7 ± 1)%, and the nitrogen concentration was obtained by nuclear reaction analysis from the number of α particles generated by the reaction of a normally incident beam of 1.15-MeV $^2H^+$ particles with the sample ($^{14}N + {}^2H^+ \rightarrow {}^4He^+ + {}^{12}C$). The nitrogen concentration x of the $Tb_{25}Fe_{68}Co_7N_x$ samples presented in this paper ranges between 0 and 6.

III. MAGNETIZATION MEASUREMENTS

The macroscopic magnetization measurements were performed in a vibrating sample magnetometer (VSM) between 10 K and 300 K, with the applied magnetic field perpendicular to the film plane. The temperature dependences of the total magnetization (M_s) and coercive field (H_c) were deduced from the hysteresis loops obtained at various temperatures.

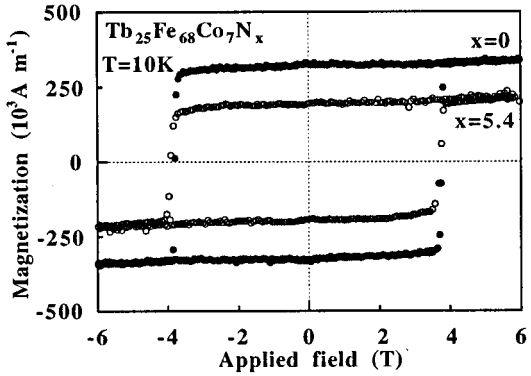

FIG. 1. Hysteresis loops of $Tb_{25}Fe_{68}Co_7$ and $Tb_{25}Fe_{68}Co_7N_{5.4}$ films at 10 K with the external field applied perpendicularly to the film plane.

Typical magnetization curves at 10 K are presented in Fig. 1 for $Tb_{25}Fe_{68}Co_7$ and $Tb_{25}Fe_{68}Co_7N_{5,4}$. The squareness of the hysteresis loops of the nitrided samples indicates that the easy axis of $Tb_{25}Fe_{68}Co_7N_x$ thin films remains perpendicular to the film plane in this composition range ($x \leqslant 6$). However, the thermal variation of the coercive field is changed by nitrogenation. Instead of decreasing monotonously with increasing temperature between 10 and 300 K as for $x=0$, the coercivity of the nitrided samples starts increasing again, at lower and lower temperature, as x increases (Fig. 2). In addition, the saturation magnetization at all temperatures is decreased by nitrogen insertion, as shown in Fig. 3. These changes in the magnetic behavior of the nitrided samples suggest that the compensation temperature is decreased by nitrogenation. The compensation and Curie temperatures (T_{comp} and T_c), experimentally determined by polar magneto-optical Kerr effect (PMOKE), are both found to decrease linearly as a function of x , but T_c is much less affected than T_{comp}. T_c and T_{comp} are presented in Fig. 4, together with the saturation magnetization (M_s) at 10 K, as a function of the nitrogen concentration x. We notice that the relative variation of the low-temperature magnetization is of

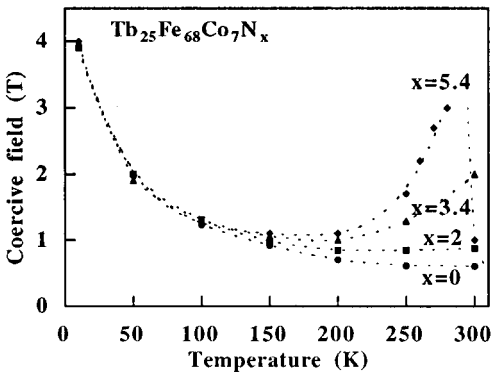

FIG. 2. Temperature dependence of the coercive field of $Tb_{25}Fe_{68}Co_7N_x$ films for various nitrogen concentrations x. The lines are only a guide for the eye.

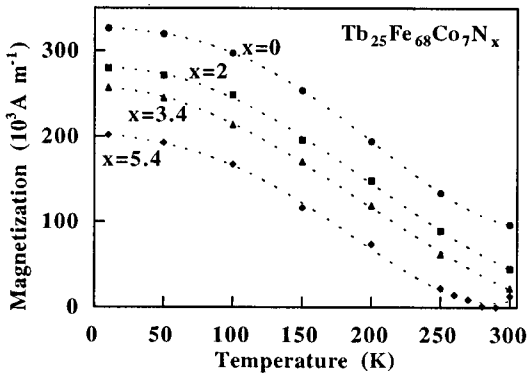

FIG. 3. Temperature dependence of the saturation magnetization of $Tb_{25}Fe_{68}Co_7N_x$ films for various nitrogen concentrations x. The lines are only a guide for the eye.

the same order of magnitude as for TbFeN.[5]

In order to determine the exact source(s) of these macroscopic phenomena, atom-specific techniques are needed. XMCD was performed on Tb and Fe, and Mössbauer spectroscopy on Fe.

IV. XMCD MEASUREMENTS

XMCD measurements at the Tb $M_{4,5}$ ($3d \rightarrow 4f$ transitions) and at the Fe $L_{2,3}$ edges ($2p \rightarrow 3d$ transitions) were carried out in total electron yield (TEY) detection on the Dragon beam line (ID12b) at the ESRF.[12] These absorption edges directly probe the electronic shells responsible for the magnetism, i.e., the RE $4f$ shell and the TM $3d$ shell. Three samples with nitrogen concentrations $x=0$, $x=3.5$, and $x=5$ were investigated at 20 K with a perpendicular applied field of 5 T. The Fe $L_{2,3}$-edge spectra were also measured in a field of 0.2 T. The samples were positioned in the UHV chamber (pressure $<10^{-9}$ Torr) of a superconducting magnet system, with the sample surface oriented perpendicular to the light propagation direction. In this geometry, XMCD probes the average Fe $3d$ and Tb $4f$ magnetic moments projected along the anisotropy axis (perpendicular to the film plane). It has been proved that the angular saturation effects intrinsic to the TEY detection are negligible in this experimental configuration.[13–15]

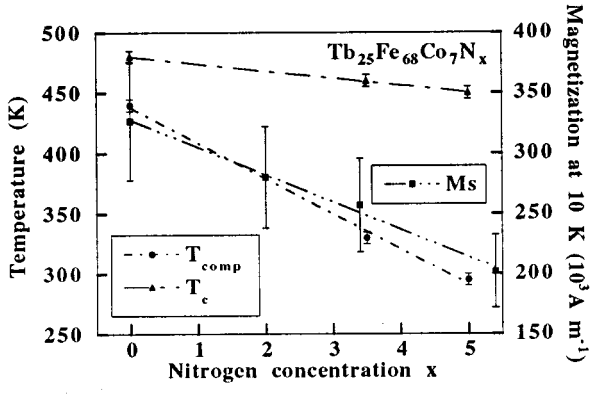

FIG. 4. Curie temperature, compensation temperature, and saturation magnetization at 10 K of $Tb_{25}Fe_{68}Co_7N_x$ films are plotted as a function of the nitrogen concentration x. The lines are linear fits to the data.

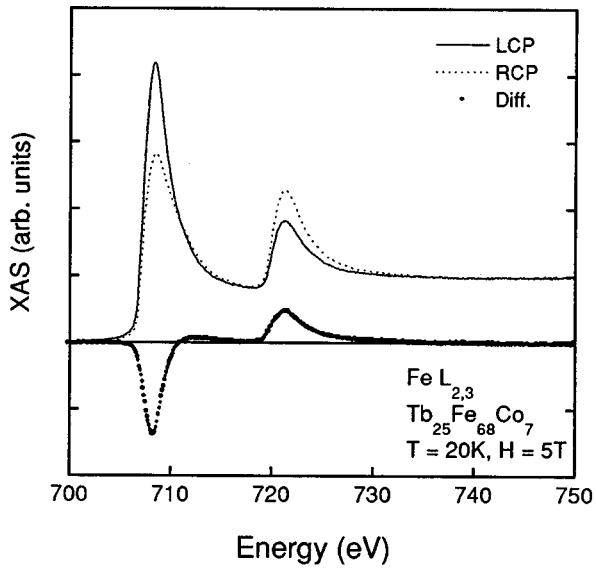

FIG. 5. Fe $L_{2,3}$ XAS spectra and XMCD spectrum measured for the nitrogen-free $Tb_{25}Fe_{68}Co_7$ sample at 20 K under an applied magnetic field of 5 T.

XMCD spectra were obtained as the difference between two absorption spectra measured with opposite x-ray-beam helicities (σ^+ and σ^-) and a fixed magnetic field direction. The helicity of the x-ray beam was changed by reversing the phase of the helical undulator. The measured rate of circular polarization is $(84\pm5)\%$ at the Fe edges[16] and about 90% at the Tb edges. The value of the polarization rate for the Fe $L_{2,3}$ edges is measured, while the one for Tb $M_{4,5}$ has been extrapolated using these data. This extrapolated value agrees well with calculations.

A. Fe $L_{2,3}$ edges

The Fe $L_{2,3}$-edge σ^+ and σ^- spectra measured for the non-nitrided sample with an applied magnetic field of 5 T are shown in Fig. 5, together with the corresponding XMCD signal. The spectra measured for the other samples are very similar. In order to extract from the XMCD signals an approximate value of the Fe $3d$ moments, we have compared the asymmetry ratio $(\sigma^+ - \sigma^-)/(\sigma^+ + \sigma^-)$ at the L_3-edge white line maximum with the asymmetry ratio obtained by Chen *et al.*[17] for an Fe thin film measured in transmission geometry with comparable resolution. Taking into account the circular polarization rate of 84%, the asymmetry ratio obtained for the spectra measured under 5 T is of the order of 23% for the sample with $x=0$ and $x=3.5$, and 24% for that with $x=5$, instead of 28% for metallic Fe. By scaling these values to the magnetic moment of bulk Fe ($2.2\mu_B$), the projected Fe moment ($\mu_{\mathrm{Fe}}^{\perp}$) is approximately $1.81\mu_B$ for $x=0$ and $x=3.5$, and $1.84\mu_B$ for that with $x=5$. The moments obtained under a magnetic field of 0.2 T are very similar. This is not surprising because the molecular field acting on the Fe moments is of the order of 600 T. The results are summarized in Table I.

TABLE I. The projections along the normal to the film plane (total magnetization direction) of the Fe $3d$ and Tb $4f$ magnetic moments obtained by XMCD at 20 K under an applied magnetic field B_0 are presented for various nitrogen concentrations together with the mean opening angle of the cone formed by the Tb moments with respect to the total magnetization direction.

	$B_0 = 0.2$ T	$B_0 = 5$ T	$B_0 = 5$ T	
x	$\mu_{Fe}^{\perp}$ (μ_B)	$\mu_{Fe}^{\perp}$ (μ_B)	$\mu_{Tb}^{\perp}$ (μ_B)	θ_{Tb} (deg)
0	1.77± 0.1	1.81 ± 0.1	6.9 ± 0.3	40± 2
3.5	1.74	1.81	6.2	46
5.0	-	1.84	5.4	53

Another way of estimating the $3d$ magnetic moments from the XMCD data consists in the use of the sum rules, introduced by Thole *et al.*[9] Although the error bar on the magnetic moments calculated by this method is rather large ($\sim$ 20%), the Fe moment that we evaluate for the sample with $x=0$ is around $(1.8 \pm 0.3)\mu_B$, which is consistent with the first method.

Whatever the method, the XMCD measurements show that the Fe moment projection hardly varies with nitrogen concentration. The main macroscopic effect of nitrogen doping — the decrease of the compensation temperature — cannot therefore be attributed to an important modification of the Fe sublattice magnetization.

B. Tb $M_{4,5}$ edges

The Tb $M_{4,5}$-edge σ^+ and σ^- spectra measured for the non-nitrided sample with an applied magnetic field of 5 T are shown in Fig. 6, as well as the XMCD signal. The signs of the Tb and Fe XMCD signals are in agreement with the antiparallel alignment of the RE and TM magnetic moments in the case of heavy RE's. The amplitude of the XMCD signal for the M_5 edge is strongly reduced as the nitrogen content is increased (Fig. 7).

In order to extract the Tb $4f$ moment from the XMCD signals, theoretical spectra were fitted to the experimental ones using the procedure described in Ref. 15. The atomic absorption spectra were calculated using the atomic multiplet program.[7,8,18] To simulate lifetime broadening, the line spectra of the atomic calculation were convoluted with a Lorentzian with a full width at half maximum (FWHM) = 0.4 eV at the M_5 edge and a Fano-like line shape with asymmetry parameter $q=9$ and FWHM = 0.8 eV for the M_4 edge. The whole spectrum was convoluted with a Gaussian line shape with a standard deviation of 0.4 eV to account for experimental resolution. The result of the best fit obtained for $x=0$ is also shown in Fig. 6.

For the Tb M_5-edge spectra measured on the non-nitrided sample, the best fit gives a projected magnetic moment of $6.9\mu_B$, taking into account the circular polarization rate of 90%. The Tb $4f$ magnetic moments obtained by this procedure for the three samples are summarized in Table I.

Because of the noncollinear structure of these amorphous alloys, the maximum value found for the Tb moment is smaller than the saturation value $(9\mu_B)$. If we assume a random distribution of the Tb moments around the field direction, the average configuration can be seen as a cone, with all the moments displayed on this cone surface. The opening angle of the cone, θ_{Tb}, is deduced from the projected Tb moment, and is indicated in Table I for each sample. Our results are consistent with those found by Vogel *et al.*[15] for a series of Tb_xFe_{1-x} amorphous alloys.

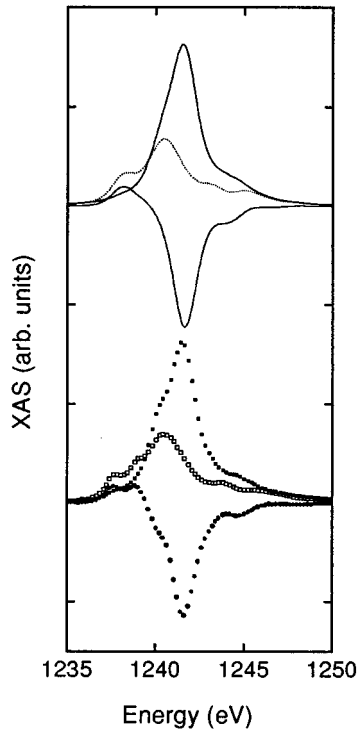

FIG. 6. Tb M_5 XAS spectra and XMCD spectrum measured for the nitrogen-free $Tb_{25}Fe_{68}Co_7$ sample at 20 K under an applied magnetic field of 5 T. Bottom: experimental spectra; (solid squares) right circular polarization; (open squares) left circular polarization; (circles) XMCD; Top: corresponding atomic multiplet simulation.

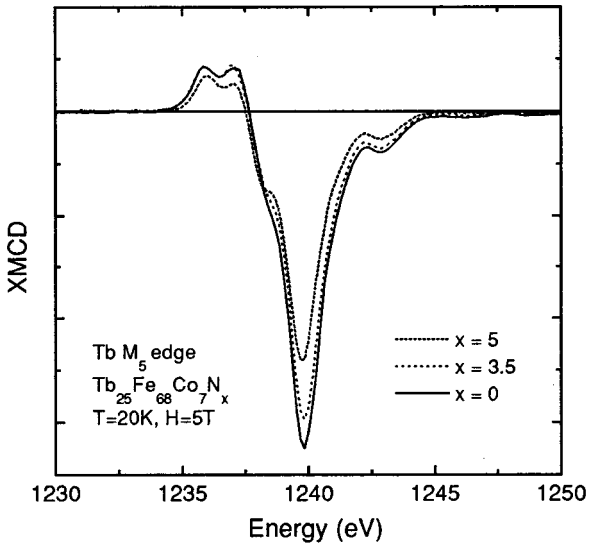

FIG. 7. Tb M_5 XMCD spectra measured for $x=0$ (solid line), $x=3.5$ (dotted line), and $x=5$ (short dotted line) at 20 K under an applied magnetic field of 5 T.

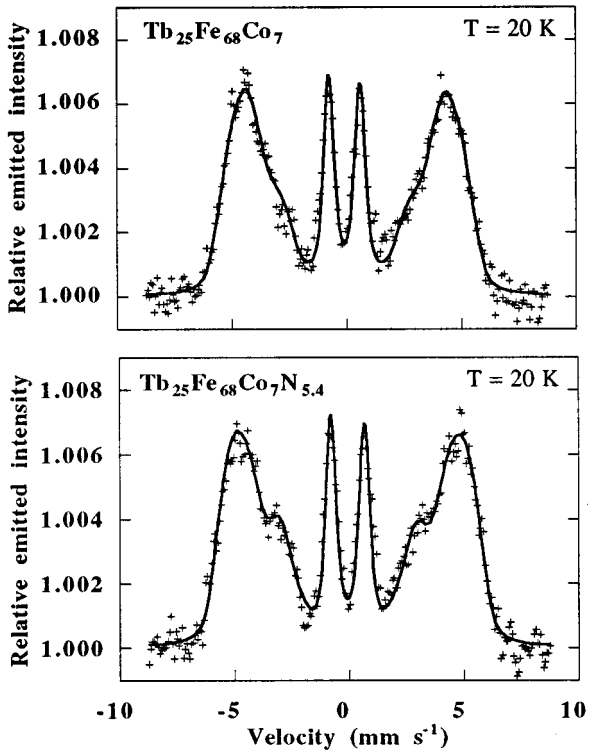

FIG. 8. CEMS spectra of $Tb_{25}Fe_{68}Co_7$ and $Tb_{25}Fe_{68}Co_7N_{5.4}$ films obtained on Fe at 20 K. The solid line is a fit to the data.

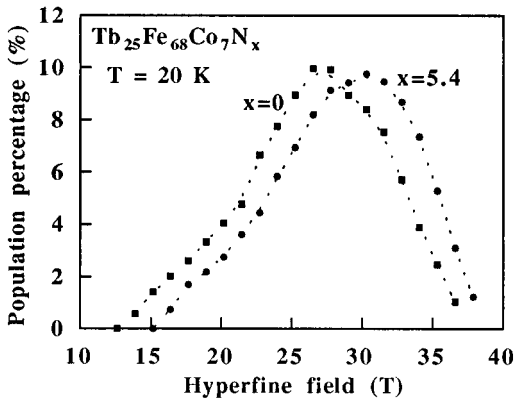

FIG. 9. Fe hyperfine field distributions obtained by CEMS for $Tb_{25}Fe_{68}Co_7$ and $Tb_{25}Fe_{68}Co_7N_{5.4}$ films at 20 K.

V. MÖSSBAUER SPECTROSCOPY MEASUREMENTS

Conversion electron Mössbauer spectroscopy (CEMS) was performed at 20 K on magnetized $Tb_{75}Fe_{68}Co_7N_x$ samples with $x=0$ and $x=5.4$, without an applied magnetic field. The radiation source was ^{57}Co in a Rh matrix, and the incident γ-ray beam was oriented perpendicular to the film plane. The spectra were fitted with a least-squares technique. Given the amorphous structure of the samples, the hyperfine field ($B_{\rm hf}$) distributions were determined using the histogram method, which imposes the width of each elementary spectrum to be the same. The Mössbauer angle between the incoming γ ray and $B_{\rm hf}$ was considered to be identical for each of the elementary spectra of the $B_{\rm hf}$ distribution. This angle, $\theta_{\rm Fe}$, representing the mean angle between the Fe magnetic moments and the normal to the film plane, was deduced from the relative intensities of the second and fifth Mössbauer lines. The isomer shift (IS), proportional to the s-electron density at the nucleus, is given relatively to α-Fe at 300 K.

The best fit to the experimental spectra (Fig. 8) was obtained using a linear correlation between $B_{\rm hf}$ and the IS. As can be seen in Fig. 9, the distribution profile of $B_{\rm hf}$ is hardly broadened by the presence of nitrogen, but mainly shifted towards higher values (+ 2 T for $x=5.4$). The magnetic field $B_{\rm hf}$ acting on the Fe nucleus is considered to be proportional to the intrinsic Fe moment ($\mu_{\rm Fe}$) carried by the $3d$ electrons. Considering the conversion factor 14.5 T/μ_B, normally used for RE-TM amorphous alloys,[19] the Fe intrinsic moment at 20 K is 1.83μ_B for $x=0$ and 1.97μ_B for $x=5.4$. The angle $\theta_{\rm Fe}$ was found to be 14° for $x=0$ and 24° for $x=5.4$. These results, together with the Fe moment projected along the perpendicular to the film plane ($\mu_{\rm Fe}^{\perp}$), the hyperfine field ($B_{\rm hf}$), the isomer shift (IS), and the width of these distributions ($\sigma_{B_{\rm hf}}$ and $\sigma_{\rm IS}$, respectively), are summarized in Table II. We notice that the presence of nitrogen significantly increases $B_{\rm hf}$, only slightly increases the IS, and does almost not affect $\sigma_{B_{\rm hf}}$ and $\sigma_{\rm IS}$. An increase in the IS is associated with a decrease in the s-electron density at the nucleus, and could be correlated either to a ''lattice'' expansion or to an $s\rightarrow d$ electronic transfer, but anyway in our case the change is too small to be significant.

VI. MEAN-FIELD ANALYSIS

In order to further give substance to this study, we have used a two-sublattice model to calculate the temperature dependence of the magnetization of Tb(Fe,Co)N alloys. As the Co concentration is low and its intrinsic moment (Co moments are collinear in RE-Co amorphous alloys) is comparable with the Fe-projected moment, Co was assimilated to Fe in the mean-field calculations. The Tb sublattice was considered in the framework of the classical HPZ model.[20] This means that to each Tb site is attributed the free-ion J value, a random anisotropy direction with a constant energy D, and

TABLE II. The hyperfine field ($B_{\rm hf}$) and the isomer shift (IS) obtained by CEMS on Fe at 20 K are presented for two nitrogen concentrations, together with their respective FWHM ($\sigma_{B_{\rm hf}}$ and $\sigma_{\rm IS}$). The Mössbauer angle $\theta_{\rm Fe}$ is also presented, as well as the intrinsic Fe magnetic moment ($\mu_{\rm Fe}$) deduced from $B_{\rm hf}$, and its projection ($\mu_{\rm Fe}^{\perp}$) along the normal to the film plane.

x	$B_{\rm hf}$ (T)	$\sigma_{B_{\rm hf}}$ (T)	$\mu_{\rm Fe}(\mu_B)$	$\theta_{\rm Fe}$ (deg)	$\mu_{\rm Fe}^{\perp}(\mu_B)$	IS (mm s^{-1})	$\sigma_{\rm IS}$ (mm s^{-1})
0	26.5 ± 0.1	11.5	1.83 ± 0.05	14 ± 2	1.77 ± 0.1	+0.060 ± 0.002	0.019
5.4	28.6	12.6	1.97	24	1.80	+0.066	0.019

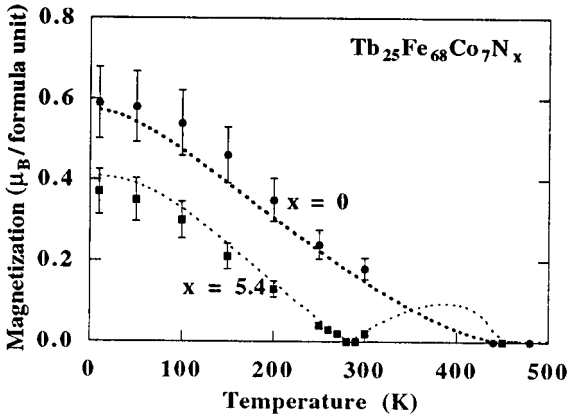

FIG. 10. Experimental temperature dependence of the saturation magnetization of $Tb_{25}Fe_{68}Co_7$ and $Tb_{25}Fe_{68}Co_7N_{5.4}$ films and mean-field calculations (dotted lines).

a uniform molecular field coming from the Fe sublattice and the mean magnetization of the Tb sublattice. The Fe sublattice magnetization is described by a Brillouin function in which the molecular field arises from the Fe-Fe interactions and also the mean Tb sublattice magnetization. The angular dispersion of the Fe moments was not modeled in the above calculations as the HPZ model is relevant only for the competition between exchange energy and local random uniaxial anisotropy energy. The Fe moment values used in the calculations are those obtained from XMCD. The use of a simple Brillouin function to describe the temperature dependence of the Fe sublattice magnetization is therefore questionable. However, the discrepancy between calculations and experimental data is small in the case of GdFe alloys.[1] The exchange and anisotropy parameters used in the program for $x=0$ ($J_{\text{Tb-Tb}}\approx 2\times 10^{-23}$J, $J_{\text{Tb-Fe}}\approx -22\times 10^{-23}$ J, $J_{\text{Fe-Fe}}\approx 47\times 10^{-23}$ J, and $D\approx 21\times 10^{-23}$ J) are close to those found elsewhere in the literature.[1,21] A 17% decrease of the Tb-Fe exchange interactions and 5% increase of the mean Fe-Fe exchange interactions enabled the experimentally observed variations of T_c and T_{comp} between $x=0$ and $x=5.4$ to be reproduced. The anisotropy energy constant D was kept fixed, whatever the nitrogen concentration, as it is difficult to imagine a radical change in the local RE environment due to such low levels of nitrogenation. The comparison between calculated and measured curves is shown in Fig. 10. The calculated values are in quite good agreement with the measurements, given the large error bars on the experimental points.

VII. DISCUSSION

The macroscopic results, summarized in Fig. 4, consist in the decrease of T_c, T_{comp}, and M_s as a function of the nitrogen concentration. XMCD and CEMS allowed these observations to be correlated with the local effect of nitrogen insertion on each magnetic sublattice. We stress that the discussion is focused on the relative variations of the various relevant parameters as a function of the nitrogen concentration, but not on their absolute values.

XMCD measurements at the Tb $M_{4,5}$ and the Fe $L_{2,3}$ edges clearly show a different behavior of the Tb and Fe sublattice magnetization as a function of nitrogen content. The low values of the projected $4f$ magnetic moment point out the existence of a noncollinear distribution of the Tb moments. The large differences observed between the XMCD signals of the three samples show that the Tb magnetic sublattice is extremely sensitive to the presence of nitrogen. The main effect of nitrogen insertion on the Tb sublattice is a decrease of its projected magnetization, which is interpreted as a modification of the noncollinear distribution of the Tb magnetic moments. As the nitrogen concentration is increased, the average opening of the conical distribution of the $4f$ Tb moments increases.

The XMCD measurements reveal that the Fe moment projected perpendicular to the film plane depends only very weakly on the nitrogen content. Unlike for Tb, we cannot assume that the intrinsic Fe moment is sample independent and thus deduce information on the angular distribution of the Fe moments. For that reason, Mössbauer spectroscopy was necessary to study the effect of nitrogen insertion on the Fe sublattice. The enhancement of the intrinsic Fe moment and the opening of the mean cone angle of the Fe moments distribution upon nitrogenation were both clearly shown by CEMS. The two effects are such that the projected Fe moment is almost constant, as also observed with the XMCD measurements. The Fe moment projections obtained by XMCD and CEMS are in very good agreement, within the experimental errors, and we stress that the field dependence between 0 and 5 T is negligible, given the order of magnitude of the molecular field acting on Fe ($\sim$ 600 T).

The modification upon nitrogenation of the angular distribution of the Tb and Fe moments can be discussed in terms of variation of the exchange interactions. Since the Tb-Tb exchange interactions are small compared to the Tb-Fe exchange interactions, the fan structure of the Tb moments mainly results from the competition between the Tb-Fe exchange interactions and the Tb local anisotropy. As the latter is intrinsic to the RE ion, the cone opening with nitrogen insertion must therefore originate from an important decrease in the Tb-Fe exchange interactions. This effect may arise from a modification of the $3d$-$5d$ orbitals overlap by nitrogen insertion.

As far as the Fe sublattice is concerned, the distribution of Fe-Fe exchange interactions gives rise, in the case of a-YFe_2, to a concentrated spin-glass behavior.[19] When Y is replaced by a magnetic RE like Tb, the presence of RE-Fe interactions reduces the effect of frustration at the different Fe sites and results in a reduced angular dispersion of the Fe moments.[21] It is thus clear that the decrease of the Tb-Fe exchange interactions upon nitrogenation, competing with the weak negative Fe-Fe interactions, will give rise to an opening of the Fe sublattice cone, as experimentally observed. The reinforcement of the intrinsic Fe moment could be the result, as for bulk intermetallic compounds, of a small lattice expansion.[22] This volume change, compatible with the slight increase of isomer shift observed by Mössbauer spectroscopy, could be small enough to be undetectable by conventional x-ray diffraction, but sufficient to lead to an increase of the Fe moment and the average $J_{\text{Fe-Fe}}$ value. This assumption has to be checked, for example, by extended x-ray-absorption fine-structure (EXAFS) measurements, on highly nitrided samples.

Although the mean-field analysis does not attempt to model precisely the magnetic behavior of these nitrided sperimagnetic alloys, the importance of the role played by the various parameters was clearly illustrated. The fact that most of the salient features of the measured data are calculated with the correct order of magnitude by simply introducing a significant decrease of $J_{\text{Tb-Fe}}$ and a slight increase of $J_{\text{Fe-Fe}}$ gives credence to the hypotheses used.

VIII. CONCLUSIONS

The study of sputtered TbFeCoN amorphous thin films shows that nitrogen insertion during deposition leads to a drastic change in the magnetic properties of the alloy, in particular the decrease of its compensation temperature. The use of element-specific probes allows us to separate the role played by nitrogen insertion on each magnetic sublattice, and mean field calculations enables us to corroborate the interpretation of the experimental data. All these techniques reveal that TbFeCo nitrogenation mainly reduces the Tb-Fe exchange interactions, slightly increases the Fe-Fe exchange interactions, and strongly enhances the Fe atomic moment.

Moreover, the flexibility of the deposition process makes it very interesting for future applications in the field of magneto-optical recording.

ACKNOWLEDGMENTS

We want to thank Y. Souche and J. F. Guillaud for their helpful contribution to the PMOKE experiments and the LETI for use of their sputtering machine. C.B. acknowledges Rhône-Poulenc for its financial support, and J. Vogel acknowledges the European Union for a grant under Contract No. ERBCHBGCT941817.

[1] P. Hansen, C. Clausen, G. Much, M. Rosenkranz, and K. Witter, J. Appl. Phys. **66**, 756 (1989).
[2] See, for a review, K. Tsutsumi and T. Fukami, J. Magn. Magn. Mater. **118**, 231 (1993).
[3] See, for example, A. Takahashi, J. Magn. Soc. Jpn. **19**, 273 (1995), and references therein.
[4] S. Hashimoto, Y. Ochiai, M. Kaneko, K. Watanabe, and K. Aso, IEEE Trans. Magn. **MAG-23**, 2278 (1987).
[5] C. Bordel, J. Voiron, and D. Givord, J. Magn. Magn. Mater. **169**, 350 (1997).
[6] C.T. Chen, F. Sette, Y. Ma, and S. Modesti, Phys. Rev. B **42**, 7262 (1990).
[7] R.D. Cowan, *The Theory of Atomic Structure and Spectra* (University of California Press, Berkeley, CA 1981).
[8] B.T. Thole, G. Van der Laan, J.C. Fuggle, G.A. Sawatzky, R.C. Karnatak, and J.-M. Esteva, Phys. Rev. B **32**, 5107 (1985).
[9] B.T. Thole, P. Carra, F. Sette, and G. Van der Laan, Phys. Rev. Lett. **68**, 1943 (1992); P. Carra, B.T. Thole, M. Altarelli, and X. Wang, *ibid.* **70**, 694 (1993).
[10] M. Sacchi, R.J.H. Kappert, J.C. Fuggle, and E.E. Marinero, Appl. Phys. Lett. **59**, 872 (1991).
[11] L.M. García, S. Pizzini, J.P. Rueff, J. Vogel, R.M. Galéra, A. Fontaine, J.P. Kappler, G. Krill, and J. Goedkoop, Appl. Phys. Lett. **79**, 6497 (1996).
[12] J. Goulon, N.B. Brookes, C. Gauthier, J. Goedkoop, C. Goulon-Ginet, M. Hagelstein, and A. Rogalev, Physica B **208**, 199 (1995).
[13] W.L. O'Brien and B.P. Tonner, Phys. Rev. B **50**, 12 672 (1994).
[14] J. Vogel and M. Sacchi, Phys. Rev. B **49**, 3230 (1994).
[15] J. Vogel, M. Sacchi, R.J.H. Kappert, J.C. Fuggle, J.B. Goedkoop, N.B. Brookes, G. van der Laan, and E.E. Marinero, J. Magn. Magn. Mater. **150**, 293 (1995).
[16] M. Drescher, G. Snell, U. Kleineberg, H.-J. Stock, N. Müller, U. Heinzmann, and N.B. Brookes, Rev. Sci. Instrum. **68**, 1939 (1997).
[17] C.T. Chen, Y.U. Idzerda, H.-J. Lin, N.V. Smith, G. Meigs, E. Chaban, G.H. Ho, E. Pellegrin, and F. Sette, Phys. Rev. Lett. **75**, 152 (1995).
[18] J.B. Goedkoop, B.T. Thole, G. van der Laan, G.A. Sawatzky, F.M.F. de Groot, and J.C. Fuggle, Phys. Rev. B **37**, 2086 (1988).
[19] J. Chappert, R. Arrese-Boggiano, and J.M. Coey, J. Magn. Magn. Mater. **7**, 175 (1978).
[20] R. Harris, M. Plischke, and M.J. Zuckermann, Phys. Rev. Lett. **31**, 160 (1973).
[21] K. Moordjani and J.M.D. Coey, *Magnetic Glasses, Methods and Phenomena* Vol. 6 (Elsevier, New York, 1984).
[22] O. Isnard, J. Alloys Compd. **205**, 1 (1994).